Phase transitions in XY models with randomly oriented crystal fields

Sumedha [1,2,*] and Mustansir Barma [3,†]

[1] *School of Physical Sciences, National Institute of Science Education and Research, Bhubaneswar, P.O. Jatni, Khurda, Odisha 752050, India*
[2] *Homi Bhabha National Institute, Training School Complex, Anushakti Nagar, Mumbai 400094, India*
[3] *TIFR Centre for Interdisciplinary Sciences, Tata Institute of Fundamental Research, Gopanpally, Hyderabad 500046, India*

(Received 5 November 2021; revised 13 January 2022; accepted 27 January 2022; published 8 February 2022)

We obtain a representation of the free energy of an XY model on a fully connected graph with spins subjected to a random crystal field of strength D and with random orientation α. Results are obtained for an arbitrary probability distribution of the disorder using large deviation theory, for any D. We show that the critical temperature is insensitive to the nature and strength of the distribution $p(\alpha)$, for a large family of distributions which includes quadriperiodic distributions, with $p(\alpha) = p(\alpha + \frac{\pi}{2})$, which includes the uniform and symmetric bimodal distributions. The specific heat vanishes as temperature $T \to 0$ if D is infinite, but approaches a constant if D is finite. We also studied the effect of asymmetry on a bimodal distribution of the orientation of the random crystal field and obtained the phase diagram comprising four phases: a mixed phase (in which spins are canted at angles which depend on the degree of disorder), an x-Ising phase, a y-Ising phase, and a paramagnetic phase, all of which meet at a tetracritical point. The canted mixed phase is present for all finite D, but vanishes when $D \to \infty$.

DOI: 10.1103/PhysRevE.105.024111

I. INTRODUCTION

Randomly anisotropic crystal fields play an important role in determining the magnetic properties of amorphous magnetic materials. In the random anisotropy model (RAM) [1], each spin is subjected to a local anisotropy with random orientation in addition to the usual spin exchange interaction. While longitudinal random anisotropy has no effect on Ising spins, for vector spins it competes with the ferromagnetic exchange energy in determining the state of the system. The model provides a theoretical basis for understanding the magnetic properties of many amorphous binary alloys [2–5] and nanocrystalline [4,6,7] and molecular [8] magnets.

The RAM can be defined for vector spins of any dimensionality $m \geqslant 2$, but in this paper we study only XY spins, corresponding to $m = 2$. In the limit of infinite strength of a crystal field oriented randomly, the model reduces to a quenched random-bond Ising model with correlated random couplings [9], raising the possibility of a spin glass phase in the RAM. In this limit, the model was conjectured to belong to the same universality class as the Edwards-Anderson Ising spin glass model [10].

Since its introduction, the model has been studied using many techniques such as mean-field theory [11–13], variational methods [14], field theories [5,15–18], and Monte Carlo simulations [19–22]. The infinite crystal field limit has been studied extensively [9,13,22–25] both analytically and through simulations using the mapping to random-bond Ising models [9]. Most ϵ expansion and Monte Carlo studies in three dimensions have been inconclusive in determining the nature of the low temperature phase. An intriguing feature of all the ϵ-expansion based renormalization group studies is that the stable fixed points cannot be reached from the initial conditions given by unrenormalized physically relevant effective Hamiltonians [17,26]. In general, the distribution of the random axis plays a crucial role in determining the low energy configurations and phase transitions.

We study the effect of random crystal field anisotropy on XY spins (RCXY) on a fully connected graph, for any distribution of the orientation of the crystal field axis and any strength of the crystal field D, using large deviation theory (LDT) [27,28]. In recent related work on fully connected graphs, LDT was used to perform the disorder averaging for discrete-spin random-field problems [29–32]. For vector spins, LDT was used to solve the problem in the pure case [33], and more recently to study XY models in random magnetic fields [34].

In this paper we use LDT to obtain the phase diagram and low temperature properties of the XY model with quenched uniform and bimodal distributions for the orientation of the crystal field. Earlier the model had been solved in the case $D = \infty$ [13]. Our solution for arbitrary D brings out an unexpected invariance of the critical temperature T_c: For a large family of distribution functions of the orientation (which includes the uniform and symmetric bimodal cases) there is a continuous transition at temperature $T_c = 1/2$, which coincides with T_c for the pure XY model on a fully connected graph, even though the nature of the ordered phase depends on the details of the disorder distribution. Below we briefly discuss the two cases studied in this paper, namely, the uniform and bimodal distributions of random orientations.

*sumedha@niser.ac.in
†barma@tifrh.res.in

In amorphous alloys, the absence of the crystalline order implies there is no preferred direction for the crystal field and the system is often modeled as the RCXY model with a uniform distribution of the random axis orientation. In this case, we find that the $T = 0$ magnetization decreases as D increases, approaching a finite value $2/\pi$ as $D \to \infty$ with a correction proportional to $1/D$ for large but finite D. Further the specific heat vanishes if $D \to \infty$, in agreement with earlier results [13], but we show that it approaches a constant as $T \to 0$ for finite values of D.

We also study an asymmetric bimodal distribution of the orientation, with the crystal field pointing randomly along x and y directions on different fractions of sites, interpolating between the pure case and the quadriperiodic bimodal distribution. An interesting phase diagram ensues with three ordered phases: two phases where the magnetization is along only one of the x or y directions, and a mixed phase with a magnetization that is canted in two different directions. Four critical curves meet at a tetracritical point which occurs for all asymmetric bimodal distributions of the random crystal field orientation. Tetracritical points have also arisen in several other contexts where there are two order parameters, for instance anisotropic antiferromagnets [35], alloys of materials with different anisotropies [36], strongly correlated SO(5) superconductors [37,38], and other strongly correlated theories like quantum chromodynamics [39]. In the RCXY model under study here, the tetracritical point originates from the asymmetric discrete distribution of the crystal field, which produces an x-y asymmetry between order parameters.

The plan of the paper is as follows: In Sec. I we define the model and derive the expression of the rate function using the large-deviation theory, for any distribution of the quenched random orientation of the crystal field. We study the phase diagram and low temperature phase for the case of uniform distribution (Sec. III) and bimodal distribution (Sec. IV), obtaining a closed form expression for the rate function as $D \to \infty$, and an expression for large D, in powers of $1/D$. We study finite D via Taylor expansion of the rate function. In Sec. V we discuss the main results of the paper and some future directions.

II. RANDOM CRYSTAL FIELD *XY* MODEL

The Hamiltonian of the model on a fully connected graph is

$$H = -\frac{J}{2N}\left(\sum_{i=1}^{N}\vec{s}_i\right)^2 - D\sum_{i=1}^{N}(\vec{n}_i\cdot\vec{s}_i)^2, \tag{1}$$

where s_i are m-component vector spins in general. For $m = 2$ (XY model), they can be represented as $s_i = \cos\theta_i\hat{i} + \sin\theta_i\hat{j}$. Here θ_i is a random variable chosen uniformly from the interval $[0, 2\pi]$, D is the crystal field strength, J is the coupling which we take to be 1, and $\hat{n}_i = \cos\alpha_i\hat{i} + \sin\alpha_i\hat{j}$ is the site dependent direction of the crystal field. The coupling between pairs of spins has been set equal to unity. The Hamiltonian depends only on the orientation of the crystal field and hence we need to consider α only on the half circle (α and $\pi + \alpha$ are equivalent). The direction of the crystal field at each site is chosen randomly and frozen; each α_i is an independent and identically distributed (i.i.d.) chosen from a specified distribution, $p(\alpha)$. The ferromagnetic coupling term in Eq. (1) tries to align spins in the same direction while the crystal field term tries to align spins with their random anisotropy axis (see Fig. 1), leading to frustration. We take D to be positive, except for the pure case (no disorder), for which we allow either sign.

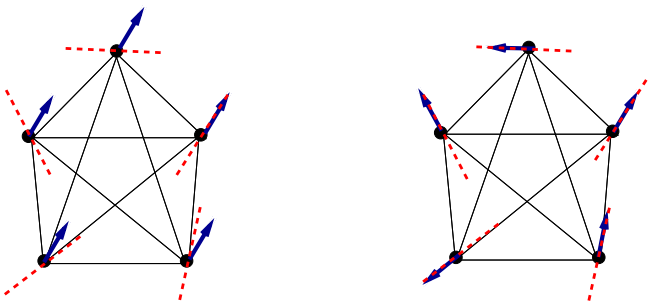

(a) (b)

FIG. 1. Low energy states with (a) $J \to \infty$ and (b) $D \to \infty$ on a fully connected graph with $N = 5$ (five spins). Spins are represented by blue arrows and the random anisotropy axes by dotted red lines. In (a) the spins align with each other while in (b) the spins align with the random anisotropy axes.

We study different forms of $p(\alpha)$ and their consequences in the subsequent sections. We use large deviation theory to perform the quenched disorder average and obtain the free energy of the model defined by Eq. (1) as explained below.

A. Calculation of the free energy functional using LDP

Consider any random configuration C_N of N spins with $x_1 = \sum_{i=1}^{N}\cos\theta_i/N$ and $x_2 = \sum_{i=1}^{N}\sin\theta_i/N$. The probability of occurrence of this configuration $P_{H,\beta}$ is proportional to $\exp(-\beta H)$, where $\beta = 1/T$. The random variables $(\sum_{i=1}^{N}\cos\theta_i, \sum_{i=1}^{N}\sin\theta_i)$ satisfy the large deviation principle (LDP) [27,28,40] with respect to $P_{H,\beta}$. This implies that there exists a rate function $I(x_1, x_2)$ such that

$$P_{H,\beta}(C_N : x_1, x_2) \sim \exp\left[-NI(x_1, x_2)\right]. \tag{2}$$

The rate function $I(x_1, x_2)$ is like the generalized free energy functional in that its minima give the free energy of the system. Recently the rate function was calculated exactly for discrete spin models with quenched random fields such as the random-field Ising model and the random crystal field Blume-Capel model defined on a fully connected graph. It was shown that the rate function when expanded in a power series is like a Landau free energy and hence can be used to extract the phase transitions in the system [29–31]. The extension of the method to vector spins, outlined below, was carried out for the random-field XY model [34].

There are two principal steps:

(1) Using the Gärtner-Ellis theorem [27,28] and the law of large numbers, we first calculate the rate function $R(x_1, x_2)$ associated with the noninteracting part of the Hamiltonian in Eq. (1) denoted by H_{ni} and given by

$$H_{ni} = -D\sum_{i=1}^{N}(\cos\theta\ \cos\alpha_i + \sin\theta\ \sin\alpha_i)^2. \tag{3}$$

Then $R(x_1, x_2)$ is defined through

$$P_{H_{ni},\beta}(C_N : x_1, x_2) \sim \exp\left[-NR(x_1, x_2)\right]. \tag{4}$$

As we will see later in this section, the rate function $R(x_1, x_2)$ becomes independent of the specific realization of the disorder and depends only on $p(\alpha)$ in the limit $N \to \infty$.

(2) The probability $P_{H,\beta}(C_N : x_1, x_2)$ for the Hamiltonian in Eq. (1) is proportional to $\int_A e^{Nf(x_1,x_2)} P_{H_{ni},\beta}$, where A is the subset of the all possible configurations, with a given (x_1, x_2). The function $f(x_1, x_2) = \beta(x_1^2 + x_2^2)/2$. The tilted large deviation principle [40] then connects the two rate functions $I(x_1, x_2)$ and $R(x_1, x_2)$ through the relation

$$I(x_1, x_2) = R(x_1, x_2) - \frac{\beta x_1^2}{2} - \frac{\beta x_2^2}{2} - \inf_{y_1,y_2}\left(R(y_1, y_2) - \frac{\beta y_1^2}{2} - \frac{\beta y_2^2}{2}\right). \tag{5}$$

The probability measure $P_{H,\beta}(C_N : x_1, x_2)$ is the tilted version of $P_{H_{ni},\beta}(C_N : x_1, x_2)$.

Let us first calculate the rate function $R(x_1, x_2)$. Using the Gärtner-Ellis theorem it can be written as

$$R(x_1, x_2) = \sup_{y_1,y_2}\{x_1 y_1 + x_2 y_2 - \Lambda(y_1, y_2)\} \tag{6}$$

provided that the scaled cumulant generating function $\Lambda(y_1, y_2) = \lim_{N\to\infty} \Lambda_N(y_1, y_2)/N$, is differentiable [27,28]. We calculate $\Lambda(y_1, y_2)$ for arbitrary distribution of the crystal field and show that it is differentiable.

The function $\Lambda_N(y_1, y_2)$ is the log cumulant generating function for the probability distribution $P_{H_{ni},\beta}$:

$$\Lambda_N(y_1, y_2) = \ln\left\langle \exp\left(y_1 \sum_{i=1}^{N} \cos\theta_i + y_2 \sum_{i=1}^{N} \sin\theta_i\right)\right\rangle_Q. \tag{7}$$

Here $\langle\cdots\rangle_Q$ represents the expectation value with respect to the probability distribution $Q \propto e^{-\beta H_{ni}}$, which is a product measure over the probability distributions Q_i for the noninteracting spins. Since $Q_i \propto \exp[\beta D \cos^2(\theta - \alpha_i)]$, we obtain

$$\Lambda(y_1, y_2) = \lim_{N\to\infty} \frac{1}{N} \sum_{i=1}^{N} \ln S_i, \tag{8}$$

where

$$S_i = \frac{1}{\tilde{N}} \int_0^{2\pi} d\theta \exp[\beta D \cos^2(\theta - \alpha_i) + y_1 \cos\theta + y_2 \sin\theta]. \tag{9}$$

Here $\tilde{N} = \int d\theta \exp[\beta D \cos^2(\theta - \alpha)]$ is the normalization and is equal to

$$\tilde{N} = 2\pi \exp(\beta D/2) I_0(\beta D/2), \tag{10}$$

where $I_0(x)$ is the zeroth order modified Bessel function of the first kind.

B. Average over disorder

Since α_i are i.i.d.'s chosen from a distribution $p(\alpha)$, the strong law of large numbers implies that as $N \to \infty$, Eq. (8) becomes

$$\Lambda(y_1, y_2) = \int_0^{2\pi} d\alpha\, p(\alpha) \ln S. \tag{11}$$

We see that since the limit $N \to \infty$ is taken, with probability 1, Λ is the same for all disorder realizations and depends only on the distribution $p(\alpha)$.

To evaluate S, we define $z = \exp(i\theta)$ and convert the integral in Eq. (9) into a contour integral over z around a unit circle. We evaluate the integral via a Laurent series expansion of the integrand (see Appendix A). The result is

$$S(y_1, y_2) = I_0(r) + 2\sum_{j=1}^{\infty} \frac{I_j(\beta D/2)}{I_0(\beta D/2)} I_{2j}(r) \cos 2j(\phi - \alpha), \tag{12}$$

where $r = \sqrt{y_1^2 + y_2^2}$ is the absolute value of the magnetization and $\phi = \tan^{-1}(y_2/y_1)$ is its orientation. Here I_j is the jth modified Bessel function of the first kind.

Let (y_1^*, y_2^*) extremize the right-hand side of Eq. (6). Both y_1^* and y_2^* are functions of x_1 and x_2, given by the solutions of the equations:

$$x_{1,2} = \frac{\partial \Lambda(y_1, y_2)}{\partial y_{1,2}}. \tag{13}$$

The rate function $I(x_1, x_2)$ can then be written as

$$I(x_1, x_2) = g(x_1, x_2) - \inf_{x_1,x_2} g(x_1, x_2), \tag{14}$$

where

$$g(x_1, x_2) = x_1 y_1^* + x_2 y_2^* - \Lambda(y_1^*, y_2^*) - \frac{\beta\left(x_1^2 + x_2^2\right)}{2}. \tag{15}$$

In the thermodynamic limit, the probability $P_{H,\beta}(C_N : x_1, x_2)$ in Eq. (2) is dominated by the minimum of $I(x_1, x_2)$, where $\frac{\partial I}{\partial x_1} = 0$ and $\frac{\partial I}{\partial x_2} = 0$, which yields $y_1^* = \beta x_1$ and $y_2^* = \beta x_2$. Note that the rate function is like a generalized free energy functional in that its minimum $\frac{1}{\beta} \inf_{x_1,x_2} I(x_1, x_2)$ provides the free energy of the system. By substituting y_1^* and y_2^* in Eq. (14) we get

$$I(x_1, x_2) = \frac{\beta r^2}{2} - \ln I_0(\beta r) - \int_0^{2\pi} d\alpha\, p(\alpha) \times \ln\left(1 + \sum_{k=1}^{\infty} 2c_k \cos[2k(\theta - \alpha)] \frac{I_{2k}(\beta r)}{I_0(\beta r)}\right), \tag{16}$$

where $r = \sqrt{x_1^2 + x_2^2}$, $\theta = \tan^{-1}(x_2/x_1)$, and

$$c_k = \frac{I_k(\beta D/2)}{I_0(\beta D/2)}. \tag{17}$$

Equation (16) is the general expression of the free energy functional for the RCXY model on a fully connected graph for an arbitrary distribution of disorder. The free energy of the system is equal to $\frac{1}{\beta} \inf_{x_1,x_2} I(x_1, x_2)$. Here x_1 and x_2 are the magnitudes of magnetization in the x and y directions, respectively, and are the two order parameters of the system. Equation (16) is the main equation that we use to study different disorder distributions in the sections that follow.

We recover the pure XY model by setting $D = 0$, in which case Eq. (16) reduces to

$$I(x_1, x_2) = \frac{\beta r^2}{2} - \ln I_0(\beta r), \tag{18}$$

which is isotropic in x_1 and x_2 and a function of r, agreeing with [33]. The self-consistent equation for the magnetization r is

$$\beta r = \beta \frac{I_1(\beta r)}{I_0(\beta r)}. \tag{19}$$

The system has a continuous transition as can be seen by expanding the right-hand side in powers of r up to third order. We get

$$\beta r \approx \frac{\beta^2 r}{2} - \frac{\beta^4 r^3}{16}, \tag{20}$$

The transition from an XY paramagnetic state ($r = 0$) to a magnetic state ($r \neq 0$) occurs at $\beta_c = 2$ ($T = 1/2$). The magnetization grows as $r \sim \sqrt{\beta - \beta_c}$, close to β_c.

For nonzero D, the phase diagram depends on the distribution of the disorder, given by $p(\alpha)$. For continuous transitions, the coefficient of the second order term in Eq. (16) decides the location of the transition. To second order, we find

$$I(x_1, x_2) \approx \frac{\beta}{4}(2-\beta)\left(x_1^2 + x_2^2\right) - \frac{\beta^2 c_1}{2} x_1 x_2 \langle \sin 2\alpha \rangle - \frac{\beta^2 c_1}{4}\left(x_1^2 - x_2^2\right)\langle \cos 2\alpha \rangle, \tag{21}$$

where $\langle \cdot \rangle$ represents an average with respect to $p(\alpha)$. We observe that for distributions with $\langle \exp(2i\alpha) \rangle = 0$, if there is a continuous transition, it is at $\beta_c = 2$ independent of the value of D. This holds for a large class of distributions, in particular for quadriperiodic distributions defined through $p(\alpha) = p(\pi/2 + \alpha)$.

In the next two sections we study the phase diagram of the RCXY model for uniform and bimodal distributions of the crystal field disorder.

III. UNIFORM DISTRIBUTION

The uniform distribution of the anisotropy axis corresponds to

$$p(\alpha) = \frac{1}{2\pi} \ \forall \alpha. \tag{22}$$

Substituting in Eq. (16), the rate function becomes

$$I(x_1, x_2) = \frac{\beta r^2}{2} - \ln I_0(\beta r) - \frac{1}{2\pi}\int_0^{2\pi} d\alpha \times \ln\left(1 + \sum_{k=1}^{\infty} 2c_k \cos\left[2k(\theta - \alpha)\right] \frac{I_{2k}(\beta r)}{I_0(\beta r)}\right). \tag{23}$$

The integral over the disorder distribution can be performed exactly when $D \to \infty$ and also at large but finite D. We first study these two cases and then examine the case of arbitrary D by expanding the integrand in powers of r.

A. Infinite D

The limit $D \to \infty$ forces each spin s_i to point along or opposite to α_i, thus reducing it to an Ising spin along the anisotropy axis.

As $D \to \infty$ the coefficients $c_k \to 1$. Setting $c_k = 1 \ \forall k$, we get

$$I(x_1, x_2) = \frac{\beta r^2}{2} - \ln I_0(\beta r) - \frac{1}{2\pi}\int_0^{2\pi} d\alpha \times \ln\left(1 + \sum_{k=1}^{\infty} 2\cos\left[2k(\theta - \alpha)\right] \frac{I_{2k}(\beta r)}{I_0(\beta r)}\right). \tag{24}$$

The summation inside the logarithmic term can then be done exactly using the identity [41]

$$\sum_{k=1}^{\infty} \cos(2kt) I_{2k}(x) = \frac{1}{2}\left[\cosh(x\cos t) - I_0(x)\right] \tag{25}$$

leading to

$$I(r) = \frac{\beta r^2}{2} - \frac{1}{2\pi}\int_0^{2\pi} d\alpha \ln\left[\cosh(\beta r \cos\alpha)\right]. \tag{26}$$

The minimum of $I(r)$ with respect to magnetization r results in a self-consistent equation for r, given by

$$r = \frac{1}{2\pi}\int_0^{2\pi} d\alpha \cos(\alpha)\tanh(\beta r \cos\alpha). \tag{27}$$

To find β_c, we expand $I(r)$ in Eq. (26) in powers of r until the fourth order:

$$I(r) = \frac{\beta r^2}{2} - \frac{\beta^2 r^2}{4} + \frac{\beta^4 r^4}{32}. \tag{28}$$

Since the coefficient of the r^4 term is positive, β_c for the transition from an XY ferromagnetic state to a paramagnet state is found by equating the coefficient of r^2 to zero. This yields $\beta_c = 2$, the same value as for the pure XY model.

The resulting model maps to a quenched random-bond Ising model with correlated variables [9], allowing a solution for the fully connected graph [13]. The self-consistent equation for magnetization obtained above [Eq. (27)] agrees with the expression obtained in [13].

Let us examine the low temperature behavior of the system. For $T = 0$ the function $\tanh[\beta r \cos(\alpha)] = 1$ if $\cos(\alpha) > 0$ and $= -1$ if $\cos(\alpha) < 0$. Hence in this case the magnetization at $T = 0$ is

$$r_0 = \frac{2}{\pi}. \tag{29}$$

For nonzero low temperature, we use $\tanh z \approx \pm[1 - 2\exp(-2|z|)]$ to obtain.

$$r = \frac{2}{\pi} - \frac{\pi T^2}{4}. \tag{30}$$

Since the second term in Eq. (26) is a function of βr, the internal energy for this model is proportional to r^2. This implies that specific heat $C_v \sim T$ for low temperatures, vanishing as $T \to 0$.

B. Large D

To study the large D behavior, we employ the asymptotic expansion of c_k [41] in Eq. (23).

$$c_k = \frac{I_k(\beta D/2)}{I_0(\beta D/2)} \approx 1 - \frac{4k^2}{8\beta D + 1}. \tag{31}$$

Differentiating Eq. (25) twice we obtain the identity

$$-\sum_{k=1}^{\infty} 4k^2 \cos(2kt) I_{2k}(x) = \frac{1}{2}[x^2 \cosh(x\cos t)\sin 2t - x\cos t \sinh(x\cos t)]. \tag{32}$$

Using Eqs. (25) and (32) and retaining terms only of order $1/D$, the rate function becomes

$$I(r) = \frac{\beta r^2}{2} - \frac{1}{2\pi}\int_0^{2\pi} d\alpha \ln(\cosh[\beta r\cos(\alpha)]) - \frac{\beta r^2}{16\pi D}\int_0^{2\pi} d\alpha \sin^2(\alpha) + \frac{r}{16\pi D}\int_0^{2\pi} d\alpha \cos(\alpha)\tanh[\beta r\cos(\alpha)]. \tag{33}$$

For low T, the free energy functional $\phi(r) = \frac{1}{\beta} I(r)$, to leading order in T is given by

$$\phi(r) = \frac{r^2}{2} - \frac{2}{\pi} r - \frac{r^2}{16D} + \frac{Tr}{4\pi D}. \tag{34}$$

Equating $\partial\phi/\partial r = 0$, we get the equation for magnetization r as

$$r - \frac{2}{\pi} - \frac{r}{8D} + \frac{T}{4\pi D} = 0. \tag{35}$$

For $T = 0$, we find

$$r = \frac{2}{\pi}\left(1 + \frac{1}{8D}\right). \tag{36}$$

The increase proportional to $1/D$ from the $D \to \infty$ value is consistent with the $T = 0$ mean-field result of [11].

For low finite temperatures, the leading order correction to the $T = 0$ value of r is proportional to T and is given by $r = \frac{2}{\pi}(1 + \frac{1}{8D} - \frac{T}{8D})$.

Since the internal energy U is proportional to r^2, it is linear in T, implying that the specific heat C goes to a constant as T approaches zero for large finite D. This is because for $T \ll D$ the spins make excursions of low amplitude δs_i around their ground state positions, with $\langle \delta s_i^2 \rangle \ll T/D$. This "Dulong-Petit" contribution results in a finite value of C. When $D = \infty$, these excitations are forbidden, leading to $C \to 0$ as $T \to 0$. The energy spectrum develops a gap for $D = \infty$ and goes to zero continuously for all finite values of D.

C. Expansion in powers of r for finite D

When the left-hand side of Eq. (23) is expanded in powers of r, the integration over α eliminates terms which are not isotropic in x_1 and x_2 and only the terms that are functions of $r = \sqrt{x_1^2 + x_2^2}$ survive. Thus $I(x_1, x_2)$ is a function of r alone for all values of D, for uniform distribution of α. For example, the expansion to 8th order reads

$$L(r) = \frac{\beta r^2(2-\beta)}{4} + \frac{(\beta r)^4}{64}\left(1 + c_1^2\right) - \frac{(\beta r)^6}{576}\left(1 + 3c_1^2\right) + \frac{(\beta r)^8}{2}\left(\frac{11}{24\,576} + \frac{49c_1^2}{18\,432} + \frac{c_2^2}{73\,728} + \frac{3c_1^4}{4096} - \frac{6c_1^2 c_2}{3689}\right) - \cdots. \tag{37}$$

In analogy with Landau theory, we have denoted the power series expansion of $I(r)$ by $L(r)$. We observe that the terms in the expansion alternate in sign for all values of D. Close to the transition temperature, r is small and it suffices to keep second and fourth order terms. Since the latter is always positive, we locate the critical point by equating the coefficient of second order term (which is independent of D) to zero. This gives

$$\beta_c = 2 \;\forall D. \tag{38}$$

The limit $D = 0$ may be recovered on noting that the alternating series can be summed and is equal to $\ln I_0(\beta r)$ [see Eq. (18)]. The coefficients a_i, associated with the ith power of r, decrease monotonically with i and the series converges. But if D is nonzero, the montonicity of the coefficients is not retained. Their magnitude increases beyond a certain value of i which depends on D. We tabulate the coefficients up to $i = 12$ in Table I for $D = 0$, 1, 10, and 1000 at $\beta = 2$ to illustrate this. Due to poor convergence for $D \neq 0$, the series cannot be used to study the low temperature behavior. The behavior of the free energy functional changes for large r, depending on the term at which we truncate the expansion. Figure 2 shows the free energy to the 10th and 12th order for $D = 0$ and $D = 2$ for $\beta = 2.1$. The possibility of a first order transition at low temperatures cannot be completely ruled out, but in our investigation until order 24, we did not find any evidence of it.

TABLE I. Coefficients of r^n for different values of D at $\beta = 2$ in Eq. (37).

D	a_4	a_6	a_8	a_{10}	a_{12}
0	0.25	−0.1111	0.0573	−0.0317	0.01825
1	0.3717	−0.2734	0.2423	−0.2361	0.2443
10	0.4875	−0.4277	0.4487	−0.5169	0.6321
1000	0.4998	−0.4443	0.4719	−0.5507	0.6819

IV. BIMODAL DISTRIBUTION

Now consider the distribution

$$p(\alpha) = p\delta(\alpha - 0) + (1-p)\delta(\alpha - \pi/2), \tag{39}$$

i.e., a fraction p of the spins experience a crystal field pointing along the x axis, while the remaining fraction $(1-p)$ are in a crystal field along the y axis. The cases $p = 0$ and $p = 1$ correspond to no disorder.

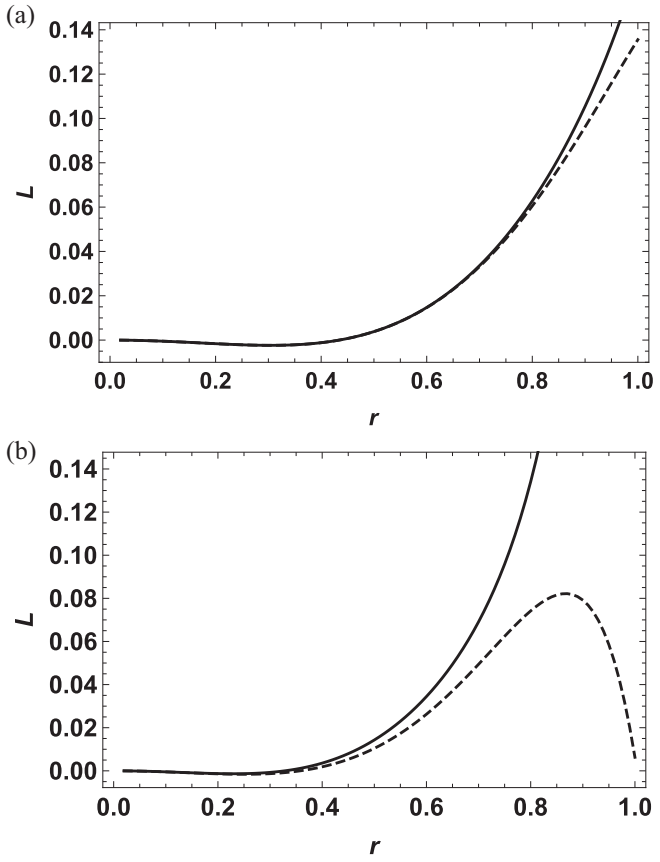

FIG. 2. Truncated Landau functional for uniform distribution obtained by expanding until 10th (12th) power in r shown as the dotted (solid) line, for (a) $D = 0$ and $\beta = 2.1$; (b) $D = 2$ and $\beta = 2.1$.

Substituting in Eq. (16), the rate function is

$$I(x_1, x_2) = \frac{\beta r^2}{2} - \ln I_0(\beta r) - p \ln\left(1 + \sum_{k=1}^{\infty} 2c_k \cos(2k\theta)\frac{I_{2k}(\beta r)}{I_0(\beta r)}\right) - (1-p)\ln\left(1 + \sum_{k=1}^{\infty} 2c_k \cos[k(\pi - 2\theta)]\frac{I_{2k}(\beta r)}{I_0(\beta r)}\right), \tag{40}$$

where again $r = \sqrt{x_1^2 + x_2^2}$, $\theta = \tan^{-1} x_2/x_1$, and $c_k = I_k(\beta D/2)/I_0(\beta D/2)$. The minimum of this function for a given set of parameters p, β, and D gives the free energy of the model.

We first discuss the phase diagram of the model in the limit of $D \to \infty$, in which case the summations inside the logarithmic term can be performed.

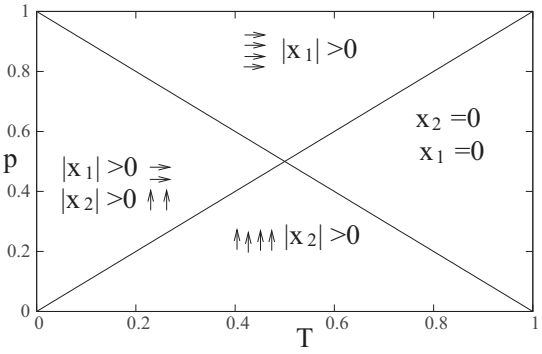

FIG. 3. p-T phase diagram for bimodal distribution for infinite D.

A. $D = \infty$

We obtain the rate function by making use of Eq. (25) in Eq. (40), with $c_k = 1$. We get

$$I(x_1, x_2) = \frac{\beta(x_1^2 + x_2^2)}{2} - p \ln[\cosh(\beta x_1)] - (1-p)\ln[\cosh(\beta x_2)]. \tag{41}$$

Minimizing the rate function gives two self-consistent equations for the order parameters in x and y directions as

$$x_1 = p \tanh \beta x_1, \tag{42}$$

$$x_2 = (1-p)\tanh \beta x_2. \tag{43}$$

For $0 \leqslant p \leqslant 1$, the RCXY model reduces to two uncoupled Ising models, with a fraction p of spins along the x direction ($x_1 = p$) and fraction $1 - p$ of spins aligned along the y direction ($x_2 = 1 - p$) in the ground state. In the p-T plane, there are two lines of continuous transitions, one with $T = p$ (separating $x_1 = 0$ from $x_1 \neq 0$) and the other with $T = (1 - p)$ (separating $x_2 = 0$ from $x_2 \neq 0$). The phase diagram has four phases as shown in Fig. 3. These phases are separated by four critical lines, all of which lie in the mean-field Ising universality class. These lines intersect at $(T, p) = (\frac{1}{2}, \frac{1}{2})$. For $T < 1/2$ the phase between the critical lines $p = T$ and $1 - p = T$ is a mixed phase with $x_1 \neq 0$ and $x_2 \neq 0$, with a total lack of coupling.

B. Finite D

For arbitrary D near the critical loci, we expand $I(x_1, x_2)$ in Eq. (40) in powers of x_1 and x_2 as they are small. This then gives us the Landau free energy expansion of the functional with known coefficients.

The lowest order term in expansion of $I_{2k}(\beta r)/I_0(\beta r)$ is of order r^{2k}. Hence the expression $\cos(2k\theta)\frac{I_{2k}(\beta r)}{I_0(\beta r)}$ has terms of order higher than four for $k > 2$. We expand Eq. (40) by keeping terms only until $k = 2$.

The result is a two parameter Landau functional of the form

$$L(x_1, x_2) = a_+(x_1^2 + x_2^2) + a_-(x_1^2 - x_2^2) + u_1 x_1^4 + u_2 x_2^4 + 2u_{12} x_1^2 x_2^2. \tag{44}$$

We denote this function by $L(x_1, x_2)$ to distinguish it from the full rate function $I(x_1, x_2)$. Here,

$$a_+ = \frac{\beta}{4}(2-\beta),$$
$$a_- = (1-2p)\frac{\beta^2 c_1}{4},$$
$$u_1 = \frac{\beta^4}{192}\left[3 - c_2 + 6c_1^2 + 8(2p-1)c_1\right],$$
$$u_2 = \frac{\beta^4}{192}\left[3 - c_2 + 6c_1^2 - 8(2p-1)c_1\right],$$
$$u_{12} = \frac{\beta^4}{64}\left(1 + c_2 - 2c_1^2\right). \quad (45)$$

The phase diagram resulting from this functional is worked out in detail in Appendix B; it depends on the value of the ratio s, defined as $s = \frac{u_1 u_2}{u_{12}^2}$. Here we merely summarize the results. There are four possible states: (0,0), $(0, x_2)$, $(x_1, 0)$, and (x_1, x_2). For $s \leqslant 1$, the phase (x_1, x_2) is not stable and the system exhibits two curves of continuous transitions given by the equations $a_+ = a_-$ and $a_+ = -a_-$. These two meet at the point $(a_+, a_-) = (0, 0)$ in the (a_+, a_-) plane. This point is a bicritical point. It is also an end point of a first order spin flop line separating the two Ising ordered phases with finite magnetizations in the x and y directions, respectively (transverse and longitudinal Ising phases, respectively). For $s > 1$, all four phases are possible and the phase diagram now has four critical curves meeting at $(a_+, a_-) = (0, 0)$. This point is now a tetracritical point.

We now use these results to obtain the phase diagram of the bimodal RCXY defined by Eq. (40) as a function of D, T, and p.

1. Pure case ($p = 0$)

For $D = \infty$ there is a transition to the longitudinal Ising phase at $T = 1$, as discussed in Sec. IV A. For finite D the coefficient of the $x_1^2 x_2^2$ term in Eq. (44) is not zero; x_1 and x_2 are coupled to each other in general.

The ratio $s = \frac{u_1 u_2}{u_{12}^2}$ in this case is 1 for $D = 0$ and decreases with increasing D. Hence the mixed phase (x_1, x_2) is not stable and the system has a bicritical point where the two critical curves meet. These two critical curves are given by $a_+ = a_-$ and $a_+ = -a_-$. They separate the paramagnetic phase from the Ising phase aligned longitudinally [] and transversely $[(x_1, 0)]$, respectively. The equations of the critical curves are

$$2 - \beta_c = \pm \beta_c c_{1,c}, \quad (46)$$

where $\beta_c = 1/T_c$ and $c_{1,c} = I_1(\beta_c D/2)/I_0(\beta_c D/2)$.

The critical curves $T_c = \frac{1 \pm c_{1,c}}{2}$ are shown in the phase diagram in Fig. 4. They separate the paramagnetic state from a state with longitudinal (transverse) order for $D > 0$ ($D < 0$). There is a first order spin flop transition on crossing the locus $T < 1/2$, $D = 0$, from a transverse to a longitudinal phase. The locus terminates in a bicritical point at $T = 1/2$, $D = 0$.

2. Quadriperiodic bimodal disorder distribution ($p = 1/2$)

We study the case $p = 1/2$ first. In this case, $a_- = 0$ and $u_1 = u_2$. Also $s = (u_1 u_2)/u_{12}^2$ is greater than 1 for all values

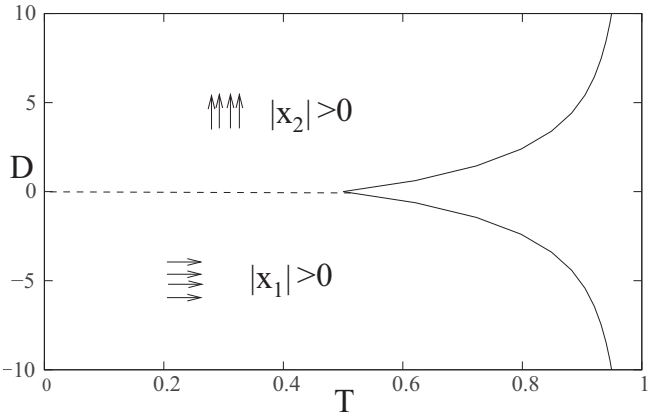

FIG. 4. Phase diagram for the pure XY model with crystal field in the y direction. The solid lines are critical curves separating the Ising phases from the paramagnetic phase. Across the dotted line there is a first order spin flop transition between the two Ising phases. As $D \to \pm\infty$, the two critical lines approach $T = 1$.

of the crystal field strength $D \neq 0$. The Landau functional in this case becomes symmetric in x_1 and x_2 and takes the form

$$L(x_1, x_2) = a_+\left(x_1^2 + x_2^2\right) + u_1 x_1^4 + u_1 x_2^4 + 2u_{12} x_1^2 x_2^2. \quad (47)$$

There is only one line of continuous transitions, given by equating a_+ to 0. This gives $\beta_c = 2$ $\forall D$. This line of continuous transition separates the XY ferromagnetic phase from a paramagnet. Hence the phase boundary in this case is the same as for the uniform distribution. However, the ordered phase is different. It is now a fourfold degenerate phase with $|x_1| = |x_2|$.

3. Asymmetric bimodal distribution, $0 < p < 1$

In this case there is a crystal field pointing in the x direction for a randomly chosen fraction p of the spins and in the y direction for the remaining fraction $1 - p$. The effect of disorder is maximum for $p = 1/2$. The ratio $s = \frac{u_1 u_2}{u_{12}^2}$ is a function of p and $w = \beta D$ alone.

For $D = 0$ and hence for $w = 0$, the ratio $s = 1$. For a fixed w, $s > 1$ for $p_l(w) < p < p_u(w)$, where $p_l(w)$ and $p_u(w)$ are functions of w alone which rapidly approach 0 and 1, respectively, as w increases (see Table II). For $p < p_l(w)$ and $p > p_u(w)$, there is no mixed phase for any value of p and T.

In the next two sections we study the phase diagram for a fixed D and fixed w separately. The phase diagram consists of

TABLE II. Lower and upper threshold on probability p such that for $p < p_l(w)$ and $p > p_u(w)$ for a given w, there is no mixed phase.

w	$p_l(w)$	$p_u(w)$
0.1	0.01582	0.98418
0.5	0.01445	0.98555
1.0	0.01107	0.98893
1.5	0.00739	0.99261
2.0	0.00449	0.99551
3.0	0.00144	0.99856

four critical curves in the p-T plane, meeting at a tetracritical point.

The two critical curves separating the (0,0) and $(0, x_2)$ phases and the (0,0) and $(x_1, 0)$ phases are given by the equations $a_+ = a_-$ and $a_+ = -a_-$, respectively. Substituting for a_+ and a_- as in Eq. (45), we get

$$T_c = \frac{[1 \pm (1 - 2p_c)c_{1,c}]}{2} \tag{48}$$

as the equations of the two critical curves, separating the transverse Ising and longitudinal Ising phases from the paramagnetic phase. Here again $c_{1,c} = I_1(\beta_c D/2)/I_0(\beta_c D/2)$.

Two other critical curves separate the $(x_1, 0)$ and $(0, x_2)$ phases from the mixed phase, represented as (x_1, x_2). They are given by $a_+ = \alpha_1 a_-$ and $a_+ = -\alpha_2 a_-$, respectively. These two conditions give the equations of critical curves to be

$$T_c = \frac{[1 \mp (1 - 2p_c)\alpha c_{1,c}]}{2}, \tag{49}$$

where $\alpha = \alpha_1 = \frac{u_1+u_{12}}{u_1-u_{12}}$ and $\alpha = \alpha_2 = \frac{u_2+u_{12}}{u_2-u_{12}}$, respectively, as defined in Appendix B. Note that u_{12}, u_1, and u_2 are also functions of p_c, D, and T_c.

4. Phase diagram with fixed D

For any finite D, as $\beta \to \infty$, $w \to \infty$, there is a mixed phase for all values of p at $T = 0$. The phase diagram has a tetracritical point at $T = 1/2$ and $p = 1/2$, where the four critical curves given by Eqs. (48) and (49) meet. The phase diagram for $D = 0.2$ and $D = 1$ in the p-T plane is plotted in Fig. 5. As D increases, the area under the mixed phase increases and the phase diagram rapidly converges to the $D \to \infty$ phase diagram given in Fig. 3. All the critical curves in the phase diagram belong to the mean-field Ising universality class as does the tetracritical point. The critical curves are straight lines only near the tetracritical point and develop nonlinearity at low temperatures, unlike the standard mean-field solutions [42].

It is instructive to examine the magnetic susceptibilities corresponding to the two order parameters x_1 and x_2. We define $\chi_{11} = (\partial x_1/\partial h_1)_{h_1 \to 0}$ and $\chi_{22} = (\partial x_2/\partial h_2)_{h_2 \to 0}$ as the susceptibilities corresponding to the magnetizations x_1 and x_2, respectively (h_1 and h_2 are the uniform external field in the directions x and y).

To study the singularities along the two different critical curves, we plot χ_{11} and χ_{22} for $p = 0.4$ for $D = 0.2$ in Fig. 6. As expected, χ_{11} diverges near the paramagnetic to Ising transition and χ_{22} diverges near the Ising to mixed phase transition. Interestingly, though, χ_{22} does not diverge near the paramagnetic to Ising transition, it exhibits a discontinuity of slope. Similar behavior is seen also for $p > 0.5$, where the roles of χ_{11} and χ_{22} are interchanged.

5. Phase diagram with fixed w

The phase diagram in the p-T plane for fixed w is similar to the phase diagram for fixed D. The main difference is at $T = 0$. For $T = 0$, with w finite, the mixed phase occurs only between two threshold values of p.

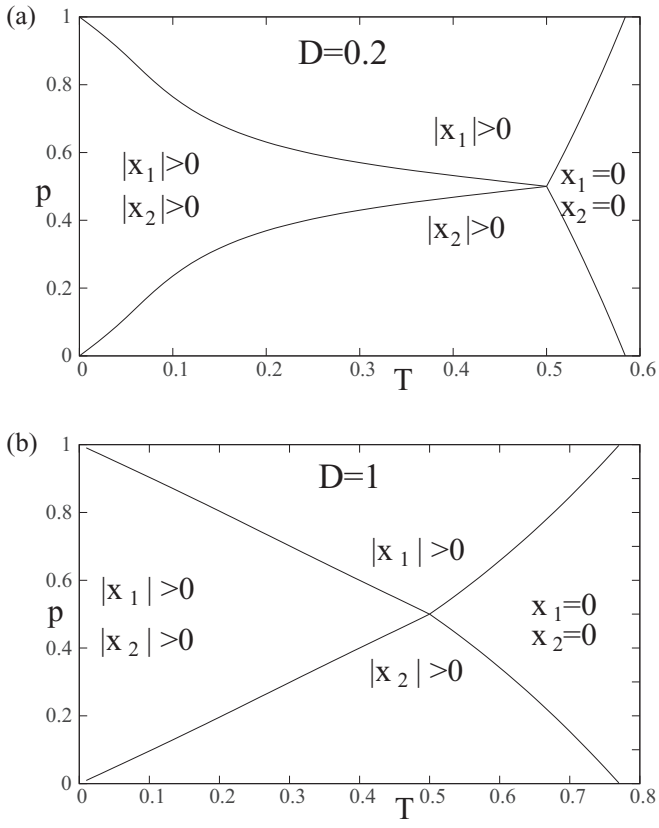

FIG. 5. Phase diagram in the p-T plane for (a) $D = 0.2$ and (b) $D = 1$ for the bimodal distribution. There is a tetracritical point at $(1/2, 1/2)$ from which four critical curves emanate, separating the four phases.

Taking $T = 0$ in Eq. (49), we find a lower threshold on p through the self-consistent equation

$$p_{0l}(w) = \frac{1}{2} - \frac{1}{2\alpha_1 c_1}, \tag{50}$$

where $p_{0l}(w)$ is the critical value of p, separating the mixed and the longitudinal Ising phases at $T = 0$. Note that $\alpha_1 =$

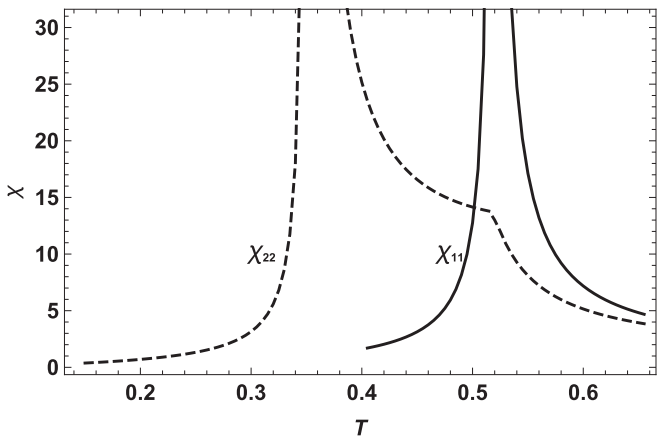

FIG. 6. Transverse (χ_{11}) and longitudinal (χ_{22}) susceptibility in the case of asymmetric bimodal distribution with $D = 0.2$ and $p = 0.4$.

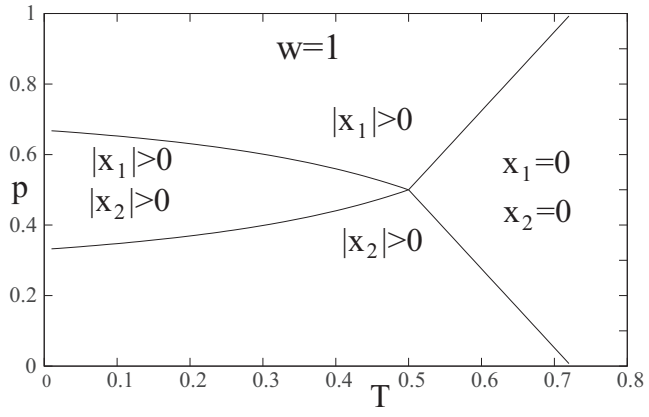

FIG. 7. Phase diagram for $w = 1$ in the p-T plane. Four critical curves meet at a tetracritical point at $(1/2, 1/2)$ for all w. The phases represented by $|x_1| > 0$ and $|x_2| > 0$ are transverse and longitudinal Ising phases with $|x_2| = 0$ and $|x_1| = 0$, respectively.

$\frac{u_1+u_{12}}{u_1-u_{12}}$ appearing on the right-hand side in Eq. (50) is also a function of $p_{0l}(w)$. The analogous upper threshold is given by

$$p_{0u}(w) = \frac{1}{2} + \frac{1}{2\alpha_2 c_1}, \tag{51}$$

where $\alpha_2 = \frac{u_2+u_{12}}{u_2-u_{12}}$.

It is instructive to plot the phase diagram in the (T, p) plane for fixed w (Fig. 7). Four critical curves meet at $p = 1/2$ and $T = 1/2$, which is thus a tetracritical point. The critical curves are straight only near the tetracritical point. The y axis intercepts $p_{0l}(w)$ and $p_{0u}(w)$ of the two critical curves approach 0 and 1, respectively, as $w \to \infty$.

As p increases, the Ising phases shrink and the critical curves approach each other. At $p = 1/2$, the critical temperature becomes independent of w and there is a single transition at $T = 1/2$ for all values of w from the disordered to the mixed phase [(0,0) to (x_1, x_2)].

C. Canted state at large D

In this ssection, we address the nature of the mixed state, and show that the magnetization vectors are canted. At $T = 0$, the exact results for $D = \infty$ in Sec. IV A give a ground state with a fraction p of spins aligned along x and a fraction $1 - p$ of spins aligned along y. On the other hand, if $D = 0$, the ground state is rotationally invariant with $r = \sqrt{x_1^2 + x_2^2} = 1$. For finite D, we use a large D expansion as in Sec. III B for the uniform distribution. Using Eq. (31) for c_k for large D in Eq. (40) and taking β to be large, the rate function reduces to

$$\begin{aligned} I(x_1, x_2) = {} & \frac{\beta}{2}(x_1^2 + x_2^2) - p\beta x_1 - (1-p)\beta x_2 \\ & - p \ln\left(1 + \frac{\beta^2 x_2^2}{1 + 8\beta D} - \frac{\beta x_1}{1 + 8\beta D}\right) \\ & - (1-p)\ln\left(1 + \frac{\beta^2 x_1^2}{1 + 8\beta D} - \frac{\beta x_2}{1 + 8\beta D}\right). \end{aligned} \tag{52}$$

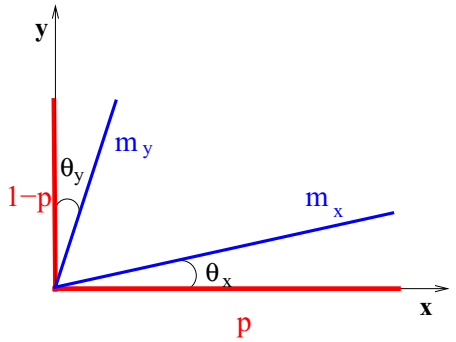

FIG. 8. The two red vectors represent the average magnetization vectors along the x and y directions for $D = \infty$ at $T = 0$, which have magnitude p and $1 - p$, respectively. Blue vectors represent the canted average magnetic vectors for large finite D at $T = 0$. We have taken p such that $p > 1 - p$ and hence $\theta_x < \theta_y$.

Keeping terms until order $1/D$, we obtain

$$\begin{aligned} I(x_1, x_2) = {} & \frac{\beta}{2}(x_1^2 + x_2^2) - p\beta x_1 \\ & - (1-p)\beta x_2 - \frac{(1-p)\beta}{8D}x_1^2 - \frac{p\beta}{8D}x_2^2. \end{aligned} \tag{53}$$

Equating partial derivatives with respect to x_1 and x_2 to 0, we obtain

$$\begin{aligned} x_1 &= p\left(1 - \frac{T}{8D} + \frac{(1-p)}{4D}\right), \\ x_2 &= (1-p)\left(1 - \frac{T}{8D} + \frac{p}{4D}\right). \end{aligned} \tag{54}$$

Equation (54) describes a state in which the magnetization vectors $\vec{m}_x$ and $\vec{m}_y$ are canted away from the x and y axes, respectively, as depicted in Fig. 8, with canting angles θ_x and θ_y (which are small for large D). To leading order in $1/D$ we may write

$$\vec{m}_x = m_x(\hat{x} + \theta_x \hat{y}); \quad \vec{m}_y = m_y(\theta_y \hat{x} + \hat{y}), \tag{55}$$

where $m_x = p$ and $m_y = 1 - p$ for $T = 0$. Comparing this with Eq. (54), we get the canting angles at $T = 0$ as

$$\theta_x = \frac{1-p}{4D}; \quad \theta_y = \frac{p}{4D}. \tag{56}$$

While the crystal field D tries to align the spins along the site with the x or y axis, depending on the value of α, the mean field produced by other spins forces canting, and the spin makes a small angle with the preferred axis.

The low T phase for finite D differs from that obtained with $D = \infty$. The specific heat shows the same behavior with the uniform distribution: it approaches zero for $D = \infty$ and is constant for finite D as $T \to 0$.

V. DISCUSSION

We studied the RCXY model for different distributions of the disorder orientation. We found a remarkable constancy of T_c for all distributions which satisfy $\langle \exp(2i\alpha) \rangle = 0$, which includes quadriperiodic distributions for which $p(\alpha) = p(\alpha +$

$\frac{\pi}{2}$). Uniform and symmetric bimodal distributions are examples of quadriperiodic distributions that we have studied in detail in this paper. In both cases, there is a single transition at $T_c = 1/2$ from a mixed magnetic phase to a paramagnetic phase. The nature of the mixed phase depends on the distribution of disorder as can be seen by looking at the disorder-averaged ground state which inherits the symmetry of $p(\alpha)$.

In the case of asymmetric bimodal distribution the asymmetry of the distribution results in a new ground state, namely, the mixed phase in which the magnetization is canted in two different directions for all finite values of the crystal field strength D. The ground state for $D = \infty$ is not canted, with spins aligned completely in the x or y direction.

We find that in general the behavior of RCXY for finite crystal field strength D is different from the behavior for $D = \infty$. The specific heat vanishes at $T = 0$ for $D = \infty$, but approaches a finite value for finite D. This is also reflected in the fact that $D = \infty$ RCXY can be mapped to the correlated random-bond Ising model [13]. We also extracted the disorder-averaged ground state of the model in the large D limit and confirmed an earlier zero temperature mean-field calculation where the order parameter at zero temperature was shown to decay as $1/D$ for uniform distribution [11].

Similar studies can be carried out for the random anisotropy model for vector spins with a number of components $m > 2$. In particular, the critical behavior can be studied easily by obtaining an expansion until fourth order in the order parameter r for uniform distribution of the disorder. This yields the critical temperature for these models to be $1/m$, independent of the strength of the crystal field on a fully connected graph. However, the full rate function needed to obtain the low temperature behavior is nontrivial due to the integrals involved in the calculation.

We have recently studied the XY model on a fully connected graph in the presence of quenched random magnetic field (RFXY) drawn from different symmetric distributions [34]. In that case, the disorder is in the field conjugate to the order parameter and has a much stronger effect. Not only T_c but also the nature of the transition changes as a function of the strength of the magnetic field. The RFXY phase diagram consists of a line of second order transitions meeting a line of first order transitions at a tricritical point. Quenched random crystal field orientation disorder, on the other hand, does not couple directly with the order parameter and has a weaker effect. As we have seen, it does not change T_c for any quadriperiodic distribution. It would be interesting to explore the quadriperiodic distribution of the random crystal field orientation on regular random graphs, in particular to see if T_c stays unchanged.

ACKNOWLEDGMENTS

S. acknowledges C. Gowdigere for discussions. M.B. acknowledges support under the DAE Homi Bhabha Chair Professorship of the Department of Atomic Energy, India.

APPENDIX A

We solve the integral in Eq. (9) using contour integration. The integral is

$$S = \frac{1}{\tilde{N}} \int_0^{2\pi} \exp[\beta D \cos^2(\theta - \alpha) + x_1 \cos\theta + x_2 \sin\theta] d\theta, \tag{A1}$$

where $\tilde{N} = \int_0^{2\pi} \exp[\beta D \cos^2(\theta - \alpha_i)]$.

We convert this integral to contour integral around a unit circle in the complex plane, by making a substitution $z = e^{i\theta}$ and $z_0 = e^{-i\alpha}$. Substituting, we get

$$S = \frac{e^{\beta D/2}}{i\tilde{N}} \oint \frac{dz}{z} \exp\left(\frac{\beta D}{4}\left(z^2 z_0^2 + z^{-2} z_0^{-2}\right)\right) \times \exp\left(\frac{x_1}{2}(z + z^{-1}) + \frac{x_2}{2i}(z - z^{-1})\right). \tag{A2}$$

We define two new variables: $a = \frac{x_1 - i x_2}{2}$ and $b = \frac{\beta D z_0^2}{4}$. The integrand in Eq. (A2) has a form $f(z)/z$, where $f(z) = \exp(bz^2 + \bar{b} z^{-2}) \exp(az + \bar{a} z^{-1})$. We can solve the integral using the residue theorem. We get $\tilde{N} S = 2\pi e^{\beta D/2} A_0$, where A_0 is the coefficient of the z^0 term in the expansion of $f(z)$. The function $f(z)$ can be expanded in terms of modified Bessel functions of the first kind as follows:

$$\exp(bz^2 + \bar{b} z^{-2}) \exp(az + \bar{a} z^{-1}) = \left(I_0(\beta D/2) + \sum_{j=1}^{\infty} [(z z_0)^{2j} + (z z_0)^{-2j}] I_j(\beta D/2)\right) \times \left(I_0(r) + \sum_{j=1}^{\infty} I_j(r) \left(\frac{2}{r}\right)^j (z^i a^j + \bar{a}^j z^{-j})\right), \tag{A3}$$

where $r = \sqrt{x_1^2 + x_2^2}$. We extracted the coefficient of the z^0 term, A_0, and it comes out to be

$$A_0 = I_0(\beta D/2) I_0(r) + \sum_{j=1}^{\infty} I_j(\beta D/2) I_{2j}(r) \times \left(\frac{2}{r}\right)^{2j} \left[(z_0 \bar{a})^{2j} + \left(z_0^{-1} a\right)^{2j}\right], \tag{A4}$$

where recall that $z_0 = e^{-i\alpha}$ and $\bar{a} = (x_1 + i x_2)/2$. We define ϕ such that $\tan\phi = x_2/x_1$. Then,

$$(z_0 \bar{a})^{2j} + (z_0^{-1} a)^{2j} = \left(\frac{r}{2}\right)^{2j} 2\cos 2j(\phi - \alpha). \tag{A5}$$

Substituting in Eq. (A4), we get

$$A_0 = I_0(\beta D/2) I_0(r) + 2 \sum_{j=1}^{\infty} I_j(\beta D/2) I_{2j}(r) \cos 2j(\phi - \alpha). \tag{A6}$$

Since $\tilde{N} = 2\pi e^{\beta D/2} I_0(\beta D/2)$, we get

$$S = I_0(r) + 2 \sum_{j=1}^{\infty} \frac{I_j(\beta D/2)}{I_0(\beta D/2)} I_{2j}(r) \cos 2j(\phi - \alpha). \tag{A7}$$

APPENDIX B

In this Appendix we study different types of phase diagrams found with the two parameter Landau functional given

in Eq. (44):

$$L(x_1, x_2) = a_+\left(x_1^2 + x_2^2\right) + a_-\left(x_1^2 - x_2^2\right) + u_1 x_1^4 + u_2 x_2^4 + 2u_{12} x_1^2 x_2^2, \tag{B1}$$

where x_1 and x_2 are the two components of the order parameter and a_+, a_-, u_1, u_2, and u_{12} are the coefficients, such that $u_1, u_2, u_{12} \geqslant 0$.

We observe that there are four possible states: (0,0), $(0, v)$, $(v, 0)$, and (v_1, v_2). The fixed points (x_1, x_2) of Eq. (B1) are obtained by equating the first derivative of $L(x_1, x_2)$ with respect to x_1 and x_2 to 0 and satisfy the following equations:

$$(a_+ + a_-)x_1 + 2u_1 x_1^3 + 2u_{12} x_1 x_2^2 = 0, \tag{B2}$$

$$(a_+ - a_-)x_2 + 2u_2 x_2^3 + 2u_{12} x_1^2 x_2 = 0. \tag{B3}$$

The stability of states can be determined by examining the Hessian at a given fixed point. The (i, j)th element of the Hessian matrix is $\partial^2 L/\partial x_i \partial x_j$. The eigenvalues of the Hessian matrix for a stable state should be $\geqslant 0$.

The general Hessian matrix for $L(x_1, x_2)$ is

$$M_H = \begin{pmatrix} a_+ + a_- + 6u_1 x_1^2 + 2u_{12} x_2^2 & 4u_{12} x_1 x_2 \\ 4u_{12} x_1 x_2 & a_+ - a_- + 6u_2 x_2^2 + 2u_{12} x_1^2 \end{pmatrix}. \tag{B4}$$

There are four possible states. The region of stability of these four states is obtained by using the condition on the eigenvalues of the Hessain as follows.

Paramagnetic phase $(x_1, x_2) = (0, 0)$. For this state Eqs. (B2) and (B3) are trivially satisfied. The Hessian is diagonal and the conditions for both eigenvalues to be positive are $(a_+ + a_-) \geqslant 0$ and $(a_+ - a_-) \geqslant 0$.

Longitudinal Ising phase $(x_1, x_2) = (v, 0)$. Fixed point equations are satisfied if

$$v^2 = -\frac{a_+ + a_-}{2u_1}. \tag{B5}$$

The phase is stable if $(a_+ + a_-) \leqslant 0$ and $a_+(1 - \frac{u_1}{u_{12}}) \geqslant a_-(1 + \frac{u_1}{u_{12}})$.

Transverse Ising phase $(x_1, x_2) = (0, v)$. Fixed point equations are satisfied if

$$v^2 = -\frac{(a_+ - a_-)}{2u_2}. \tag{B6}$$

The phase is stable if $(a_+ - a_-) \leqslant 0$ and $a_+(1 - \frac{u_2}{u_{12}}) \leqslant a_-(1 + \frac{u_2}{u_{12}})$.

Mixed phase $(x_1, x_2) = (v_1, v_2)$. Expressions of v_2^2 and v_1^2 from the fixed point equations are as follows:

$$v_2^2 = -\frac{(a_+ + a_-) + 2u_1 v_1^2}{2u_{12}}, \tag{B7}$$

$$v_1^2 = -\frac{(a_+ - a_-) - 2u_2 v_2^2}{2u_{12}}. \tag{B8}$$

The eigenvalues are

$$\lambda_\pm = \tfrac{1}{2}\left[\left(u_1 v_1^2 + u_2 v_2^2\right) \pm \sqrt{\left(u_1 v_1^2 - u_2 v_2^2\right)^2 + 4 v_1^2 v_2^2 u_{12}^2}\right]. \tag{B9}$$

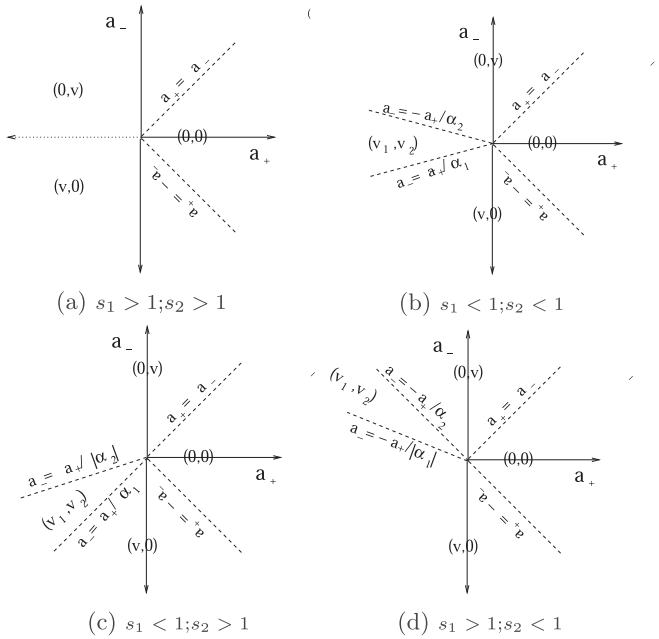

(a) $s_1 > 1; s_2 > 1$ (b) $s_1 < 1; s_2 < 1$

(c) $s_1 < 1; s_2 > 1$ (d) $s_1 > 1; s_2 < 1$

FIG. 9. Possible phase diagrams from a two parameter Landau theory. Solid line represents the coordinate axes. Dashed and dotted lines represent the locus of continuous and first order transitions, respectively. For $u_1 u_2 < u_{12}^2$, the phase diagram consists of two lines of continuous transition and a line of first order transition meeting at a bicritical point as shown in (a). For $u_1 u_2 > u_{12}^2$ there are four phases, which meet at a tetracritical point as shown in (b), (c), and (d). The topology, though, can be different depending on the ratios of $\frac{u_{12}}{u_1}$ and $\frac{u_{12}}{u_2}$.

Both eigenvalues are greater than equal to zero when

$$\frac{u_1 u_2}{u_{12}^2} \geqslant 1. \tag{B10}$$

Thus if $\frac{u_1 u_2}{u_{12}^2} < 1$, then there cannot be a mixed state in the system.

Besides the above condition, it is also required that $v_1^2 \geqslant 0$ and $v_2^2 \geqslant 0$. Solving Eqs. (B7) and (B8), we get

$$v_1^2 = \frac{a_+(u_{12} - u_2) - a_-(u_{12} + u_2)}{2\left(u_1 u_2 - u_{12}^2\right)}, \tag{B11}$$

$$v_2^2 = \frac{a_+(u_{12} - u_1) + a_-(u_{12} + u_1)}{2\left(u_1 u_2 - u_{12}^2\right)}. \tag{B12}$$

Since $v_1^2 \geqslant 0$ and $v_2^2 \geqslant 0$, we obtain two more additional conditions for the existence of the mixed phase: (1) $a_-(1 + u_{12}/u_1) \geqslant a_+(1 - u_{12}/u_1)$; and (2) $a_+(u_{12}/u_2 - 1) \geqslant a_-(1 + u_{12}/u_2)$.

We define $s_1 = u_{12}/u_1$, $s_2 = u_{12}/u_2$, $\alpha_1 = \frac{1+u_{12}/u_1}{1-u_{12}/u_1} = \frac{1+s_1}{1-s_1}$, and $\alpha_2 = \frac{1+u_{12}/u_2}{1-u_{12}/u_2} = \frac{1+s_2}{1-s_2}$. Then the condition for the existence of a mixed phase is $a_+ \leqslant \alpha_1 a_-$ and $a_+ \leqslant -\alpha_2 a_-$.

The Landau functional defined in Eq. (B1) yields four different kinds of phase diagrams, which are described below.

For $u_1 u_2 \leqslant u_{12}^2$ the state (v_1, v_2) is not possible. There are three states in the system, and the phase diagram in the

(a_+, a_-) plane has a bicritical point at (0,0); there is a first order line along the negative x axis starting at the bicritical point, separating the $(0, v)$ and $(v, 0)$ phases. The $(0, v)$ and $(v, 0)$ phases are separated from the (0,0) phase via a line of critical points along $a_+ = a_-$ and $a_+ = -a_-$, respectively, as shown in Fig. 9(a).

For $u_1u_2 > u_{12}^2$, there are four critical lines: $a_+ = a_-$, $a_+ = -a_-$, $a_+ = \alpha_1 a_-$, and $a_+ = -\alpha_2 a_-$, which meet at $a_+ = a_- = 0$ in the (a_+, a_-) plane. The phase (0,0) exists between the lines $a_+ = a_-$ and $a_+ = -a_-$. There are three different phase diagrams depending on the value of s_1 and s_2:

(1) $s_1 < 1$ and $s_2 < 1$ ($\alpha_1 > 1$ and $\alpha_2 > 1$): In this case α_1 and α_2 are both greater than 1 and the mixed phase occurs between $a_- = a_+/\alpha_1$ and $a_- = -a_+/\alpha_2$ as shown in Fig. 9(b).

(2) $s_1 < 1$ and $s_2 > 1$ ($\alpha_1 > 1$ and $\alpha_2 = -|\alpha_2|$, where $|\alpha_2| > 1$): In this case $\frac{|\alpha_2|}{\alpha_1} > 1$ and the mixed phase exists for $a_- \geqslant \frac{a_+}{\alpha_1}$ and $a_- \leqslant \frac{a_+}{|\alpha_2|}$. The phase diagram is as shown in Fig. 9(c).

(3) $s_1 > 1$ and $s_2 < 1$ ($\alpha_2 > 1$ and $\alpha_1 = -|\alpha_1|$, where $|\alpha_1| > 1$): In this case $\frac{|\alpha_1|}{\alpha_2} > 1$ and the mixed phase exists between $a_- \leqslant \frac{-a_+}{\alpha_2}$ and $a_- \geqslant \frac{-a_+}{|\alpha_1|}$. The phase diagram is as shown in Fig. 9(d).

We remark that the condition, Eq. (B10), for the existence of the mixed state was known earlier [42,43]. Besides reproducing the relation, we have shown above that the phase diagram depends also on the ratios $\frac{u_{12}}{u_1}$ and $\frac{u_{12}}{u_2}$. Here we considered only the case with $u_{12}, u_1, u_2 \geqslant 0$; negative values of u_{12} have been considered in [43].

[1] R. Harris, M. Plischke, and J. Zuckerman, Phys. Rev. Lett. **31**, 160 (1973).
[2] U. Krey, J. Magn. Magn. Mater. **6**, 27 (1977).
[3] R. Alben, J. J. Becker, and M. C. Chi, J. Appl. Phys. **49**, 1653 (1978).
[4] G. Herzer, The random anisotropy model, in *Properties and Applications of Nanocrystalline Alloys from Amorphous Precursors*, edited by B. Idzikowski, P. Švec, and M. Miglierini, NATO Science Series (Series II: Mathematics, Physics and Chemistry) Vol. 184 (Springer, Dordrecht, 2005).
[5] M. Dudka, R. Folk, and Yu. Holovatch, J. Magn. Magn. Mater. **294**, 305 (2005).
[6] A. Hernando, M. Vázquez, T. Kulik, and C. Prados, Phys. Rev. B **51**, 3581 (1995).
[7] K. L. Alvarez, J. M. Martin, N. Burgos, M. Ipatov, L. Dominguez, and J. Gonzalez, Nanomaterials **10**, 884 (2020).
[8] M. A. Girtu, C. M. Wynn, J. Zhang, J. S. Miller, and A. J. Epstein, Phys. Rev. B **61**, 492 (2000).
[9] J. H. Chen and T. C. Lubensky, Phys. Rev. B **16**, 2106 (1977).
[10] A. J. Bray and M. A. Moore, J Phys. C : Solid State Phys. **18**, L139 (1985).
[11] E. Callen, Y. J. Liu, and J. R. Cullen, Phys. Rev. B **16**, 263 (1977).
[12] J. D. Patterson, G. R. Gruzalski, and D. J. Sellmyer, Phys. Rev. B **18**, 1377 (1978).
[13] B. Derrida and J. Vannimenus, J. Phys. C: Solid State Phys. **13**, 3261 (1980).
[14] D. C. Carvalho, L. M. Castro, and J. A. Plascak, Physica A **391**, 1149 (2012).
[15] R. A. Pelcovits, Phys. Rev. B **19**, 465 (1979).
[16] D. Mukamel and G. Grinstein, Phys. Rev. B **25**, 381 (1982).
[17] D. Shapoval, M. Dudka, A. A. Fedorenko, and Yu. Holovatch, Phys. Rev. B **101**, 064402 (2020).
[18] D. Mouhanna and G. Tarjus, Phys. Rev. B **94**, 214205 (2016).
[19] R. T. S. Freire and J. A. Plascak, Phys. Rev. E **91**, 032146 (2015).
[20] B. Dieny and B. Barbara, Phys. Rev. B **41**, 11549 (1990).
[21] R. Fisch, Phys. Rev. B **79**, 214429 (2009).
[22] F. Liers, J. Lukic, E. Marinari, A. Pelissetto, and E. Vicari, Phys. Rev. B **76**, 174423 (2007).
[23] C. Jayaprakash and S. Kirkpatrick, Phys. Rev. B **21**, 4072 (1980).
[24] K. H. Fischer and A. Zippelius, J. Phys. C: Solid State Phys. **18**, L1139 (1985).
[25] R. Fisch, Phys. Rev. Lett. **66**, 2041 (1991).
[26] We thank the referee for pointing this out.
[27] A. Dembo and O. Zeitouni, *Large Deviations Techniques and Applications* (Springer-Verlag, New York, 1998).
[28] H. Touchette, Phys. Rep. **478**, 1 (2009).
[29] M. Lowe, R. Meiners, and F. Torres, J. Phys. A: Math. Theor. **46**, 125004 (2013).
[30] Sumedha and S. K. Singh, Phys. A (Amsterdam, Neth.) **442**, 276 (2016).
[31] Sumedha and N. K. Jana, J. Phys A: Math. Theor. **50**, 015003 (2017).
[32] L. P. Arguin and N. Kistler, J. Stat. Phys. **157**, 1 (2014).
[33] K. Kirkpatrick and T. Nawaz, J. Stat. Phys. **165**, 1114 (2016).
[34] Sumedha and M. Barma, J. Phys. A: Math. Theor. **55**, 095001 (2022).
[35] J. M. Kosterlitz, D. R. Nelson, and M. E. Fisher, Phys. Rev. B **13**, 412 (1976).
[36] A. Aharony and S. Fishman, Phys. Rev. Lett. **37**, 1587 (1976).
[37] S. C. Zhang, Science **275**, 1089 (1997).
[38] S. Murakami and N. Nagaosa, J. Phys. Soc. Jpn. **69**, 2395 (2000).
[39] F. Sannino and K. Tuominen, Phys. Rev. D **70**, 034019 (2004).
[40] Frank den Hollander, *Large Deviations, Fields Institute Monographs* (American Mathematical Society, Providence, 2000), Theorem III.17.
[41] M. Abramowitz, *Handbook of Mathematical Functions, with Formulas, Graphs, and Mathematical Tables* (Dover, New York, 1974).
[42] P. M. Chaikin and T. C. Lubensky, *Principles of Condensed Matter Physics* (Cambridge University Press, Cambridge, 2000).
[43] S. Watanabe and T. Usui, Prog. Theor. Phys. **73**, 1305 (1985).